ACS Photonics

Article

pubs.acs.org/journal/apchd5

Direct Observation of Multiphoton Emission Enhancement from a Single Quantum Dot Using AFM Manipulation of a Cubic Gold Nanoparticle

Sadahiro Masuo,*[,†] Keisuke Kanetaka,[†] Ryota Sato,[‡] and Toshiharu Teranishi[‡]

[†]Department of Applied Chemistry for Environment, Kwansei Gakuin University, 2-1 Gakuen, Sanda, Hyogo 669-1337, Japan

[‡]Institute for Chemical Research, Kyoto University, Gokasho, Uji, Kyoto 661-0011, Japan

Supporting Information

ABSTRACT: The change of photon statistics in the fluorescence of a single CdSe/ZnS core/shell colloidal nanocrystal quantum dot (NQD) accompanying the atomic force microscopy (AFM) manipulation of a cubic Au nanoparticle (AuCube) was investigated to elucidate the effect of plasmonic nanostructures on the multiexciton dynamics of the NQD. Upon coupling to an AuCube of a well-defined size and shape, we directly observed the conversion of a single-photon emission from an individual NQD to a multiphoton emission, and this was accompanied by an increase in fluorescence intensity and a reduction in fluorescence lifetime. The multiphoton emission then returned to a single-photon emission upon separating the AuCube from the single NQD. The efficiency of the multiphoton emission was enhanced 6.9 times through the use of the AuCube. The enhancement of the multiphoton emission was attributable mainly to the augmentation of the biexciton emission rate. These results provide evidence that quantum dot photon statistics can be manipulated by plasmonic nanostructures, and NQD-plasmonic nanostructure systems can be desirable for many technological applications.

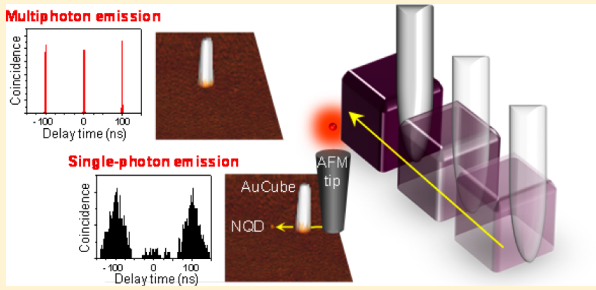

KEYWORDS: *colloidal quantum dot, plasmonics, single photon, multiphoton, AFM manipulation, metal nanoparticle*

Colloidal nanocrystal quantum dots (NQDs) are a unique class of tunable, dispersible fluorophores that are of great interest for applications in a wide range of optoelectronic devices.[1−9] An important and interesting exciton dynamics is the simultaneous existence of multiple excitons (MX) in a single NQD. MX can be generated upon the absorption of multiple photons that each have energy equal to the NQD band gap or upon the absorption of a single photon bearing at least twice the band gap energy.[10−14] The latter process is called multiple exciton generation (MEG). MEG, and the subsequent extraction of multiple carriers, represents a promising route to ultimately improve the power conversion efficiency of NQD-based photovoltaic cells.[15−19] Furthermore, the cascade emission from MX, that is, multiphoton emission from triexciton (TX) and biexciton (BX) states, is valued for its production of correlated photon pairs (also called entangled photons) to realize quantum information and communication technologies.[20]

However, when MX are generated in a single NQD, they can decay by nonradiative Auger recombination (AR), that is, the MX are reduced to a single exciton (SX) by AR[21] and are wastefully consumed. AR also causes the fluorescence blinking behavior that is known as Auger ionization.[22] Therefore, suppression of AR has been extensively studied for efficient use of the excitons.[23−26] On the other hand, AR facilitates single-photon emission for the single NQD, that is, photon antibunching in the NQD fluorescence, because the surviving SX can emit a single photon even when MX are produced in an NQD.[27−30] The single-photon emission is also an important and interesting optical property of the single NQD for quantum information and communication technologies. Therefore, it is very important to control the MX dynamics for applications employing NQDs.

We previously reported that MX dynamics, that is, the probability of a multiphoton emission from MX and a single-photon emission from SX, can be modified through interactions of the NQD with metallic nanostructures.[31−33] By applying a photon-correlation measurement to a single CdSe/ZnS core/shell NQD coupled to silver nanoparticles (AgNPs), we revealed that the quantum yield (QY) of BX emission increased when the fluorescence lifetime was shortened to the instrument response function (0.4 ns). To explain this result, we proposed that, when BX are generated in a single NQD, BX emission and AR are competitive processes. A single NQD itself emits a single-photon even when BX are generated because the rate of AR is much faster than that of BX emission. The time scale of AR depends on the volume of the NQD. In the case of our

Received: September 4, 2015
Published: December 8, 2015

DOI: 10.1021/acsphotonics.5b00496
ACS Photonics 2016, 3, 109−116

NQD (core radius: 2.6 nm), AR occurs within 100 ps.[21] In contrast, for single NQDs coupled with AgNPs, an enhanced emission of the BX occurs, and the BX emission can be emitted before AR. Therefore, a single NQD with a short lifetime (i.e., the rate of BX emission is faster than that of AR) exhibits an increase in the QY of BX emission, which also represents a decrease in the probability of photon antibunching.[31,32] These results indicate that the BX emission can be improved by the interaction with AgNPs; as a result, AR can be suppressed.

Recently, a similar enhancement of multiphoton emission was reported using combinations of CdSe/CdS-random gold[34] and silver[35,36] films, a CdSe/CdS-gold gap bar antenna structure,[37] a CdSe/ZnS-rough gold film,[38] and a CdSe/ZnS-plasmonic cavity, which consisted of a silver nanocube and a gold film.[39] These reports have clearly demonstrated an increased probability of multiphoton emission, that is, BX emission, from a single NQD via an interaction with metallic nanostructures. Two possibilities have been discussed to describe the mechanism behind these increases in the BX emission. One mechanism involves the enhancement of the BX emission rate by the metallic nanostructure, which is similar to our previous results mentioned above. Another is the quenching of SX emission by the metallic nanostructure, that is, a decrease in the QY of SX emission rather than an actual increase in the QY of BX emission[36,40,41] Thus, the interplay of NQDs and metallic nanostructures, particularly the influence of metallic nanostructures on the MX dynamics of the NQD, is not fully understood. Furthermore, the critical problem of these reports, including ours, is that the possibility of measuring a cluster of the NQDs cannot be excluded. When single NQDs are deposited onto a glass substrate or metallic film, then the individual NQDs tend to form clusters. Even when the NQDs are dispersed in a polymer thin film, such as poly(methyl methacrylate), a few tens of percents of the NQDs form clusters.[39] If a single cluster is measured in substitution of a single NQD, then the observed emission behavior can appear to be an enhancement of the multiphoton emission. To exclude this possibility and to understand the interaction between single NQDs and metallic nanostructures, one would have to directly observe changes in the emission behavior of a single NQD that accompany the interaction with a metallic nanostructure. To achieve this direct observation, atomic force microscopy (AFM) is the ideal technique to manipulate the metallic nanostructure. Indeed, changes in the emission behaviors of a single fluorescence sphere,[42] nitrogen vacancy center,[43,44] and NQD[45] approaching single metallic nanoparticles by AFM manipulation have clearly been observed in situ. However, photon statistics in the fluorescence from a single NQD utilizing AFM manipulation have never been reported.

To elucidate the possibility of controlling MX dynamics using a metallic nanostructure, that is, the MX-metallic nanostructure interaction, AFM manipulation was employed in this study (Figure 1). The change in the fluorescence photon statistics of a single NQD by an approaching cubic gold nanoparticle (AuCube) was directly observed; in other words, the single-photon emission of an individual NQD was converted to multiphoton emission by the interaction with a metallic nanostructure. This result directly indicates that the MX dynamics can be controlled by interactions with metallic nanostructures.

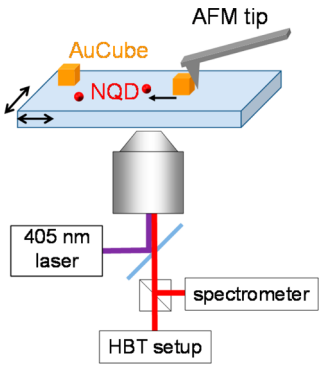

Figure 1. Schematic of the experimental setup for AFM manipulation of a single AuCube.

RESULTS AND DISCUSSION

A transmission electron microscopy (TEM) image of the AuCube is shown in Figure 2a. Monodispersed cubic Au nanoparticles (AuCube) of a well-defined size and shape were confirmed by this image. The size of the AuCube was estimated as 87 ± 2.4 nm from the TEM image. An extinction spectrum of the AuCube-dispersed aqueous solution is shown in Figure 2b with the absorption and fluorescence spectra of NQD in toluene. The localized surface plasmon resonance (LSPR) band of the AuCube overlaps with both the absorption and fluorescence spectra of the NQD. This indicates that both excitation and relaxation processes of the NQD can be enhanced with the AuCube by with choice of excitation wavelength. It is well-known that the fluorophore−metallic nanostructure interaction strongly depends on the spectral overlap and the distance between a fluorophore and a metallic nanostructure. When the absorption of the fluorophore

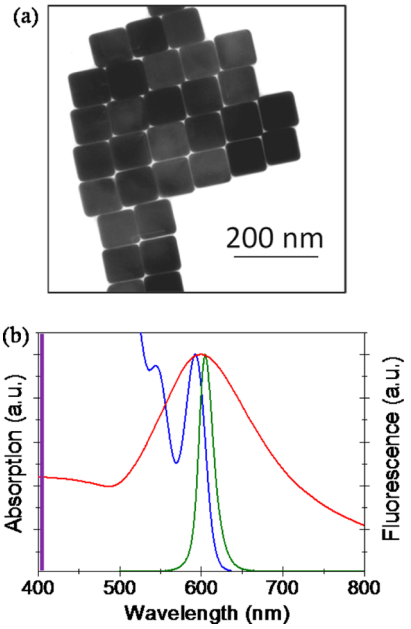

Figure 2. (a) Transmission electron microscopy image of monodispersed cubic Au nanoparticles (AuCubes). (b) An extinction spectrum of the AuCube colloidal solution (red), absorption (blue) and fluorescence (green) spectra of a CdSe/ZnS QD colloidal solution. The wavelength of the excitation laser is marked as a purple vertical line.

DOI: 10.1021/acsphotonics.5b00496
ACS Photonics 2016, 3, 109−116

overlaps with the LSPR band, the excitation rate of the fluorophore can be augmented by the electric field of the LSPR generated by the excitation light. Similarly, when the fluorescence spectrum of the fluorophore overlaps with the LSPR band, this relaxation process can be enhanced. The enhanced relaxation process is interpreted as the resonant energy transfer from the excited state of the fluorophore to the metallic nanostructure through dipole−dipole interactions; therefore, the LSPR can be generated on the metallic nanostructure by energy transfer and then decays radiatively and nonradiatively. The fluorescence lifetime (τ) and the QY (Φ) of the "fluorophore−metallic nanostructure" system can be expressed as $\tau = 1/(k_{r0} + k_{nr0} + k_{rp} + k_{nrp})$ and $\Phi = (k_{r0} + k_{rp})/(k_{r0} + k_{nr0} + k_{rp} + k_{nrp})$, where k_{r0} and k_{nr0} are the intrinsic radiative and nonradiative decay rates of the fluorophore, respectively, and k_{rp} and k_{nrp} are the radiative and nonradiative decay rates of the LSPR generated on a metallic nanostructure, respectively. When the distance between the fluorophore and the metallic nanostructure is closed, then electron transfer from the excited fluorophore to the metallic nanostructure should be considered. Under our experimental conditions, the LSPR could not be efficiently generated by the excitation laser (405 nm; Figure 2b). Therefore, the enhancement of the relaxation process was considered. The advantage of the well-defined AuCube is that there is little variation of the LSPR band in each AuCube; hence, we can simply consider the mechanism of the NQD-metallic nanostructure interaction.

Figures 3 and 4 show the representative results of AFM manipulation of an AuCube and the accompanying emission behavior that was detected from a single NQD. In the AFM images, a big white object and small white dots correspond to a single AuCube and individual NQDs, respectively. The AuCube does not appear square-shaped because the end of the AFM tip was broken during manipulation of another AuCube, which led to the large radius of curvature for the probe. When the AFM image of an AuCube was observed by an AFM tip with a sharper radius of curvature, then the square shape of the AuCube was observed (see the Supporting Information, SI). The cross-section of a single NQD and a single AuCube from the expanded view inset in Figure 3a is shown in Figure 3c. The heights of the AuCube (88 nm) and NQD (5 nm) were in good agreement with the expected values. The center-to-center distance between the NQD and the AuCube was estimated to be 185 nm. The larger width of the AuCube (160 nm) compared to its height (88 nm) was due to the large curvature of the AFM tip. In the fluorescence images, the signals from individual NQDs were collected from the same NQD positions shown in the AFM image. The blank lines observed in the fluorescence images of the single NQDs are attributable to off-periods arising from fluorescence blinking. The AuCube was then pushed in the direction of the red arrow (Figure 3a) and approached the single NQD. After moving the AuCube near the NQD, the single NQD could not be visualized in the AFM image (Figure 3d). To estimate the center-to-center distance between the NQD and AuCube, we assumed that the single NQDs were fixed before and after the manipulation of the AuCube, and the position of another single NQD was used as the reference point. By this way, the center-to-center distance was estimated as 5 nm, indicating that the NQD physically overlapped (i.e., on the top of) with the AuCube or might be attached to the side of the AuCube. In the fluorescence image taken after manipulation (Figure 3e), the blank lines, which are associated with the blinking of a single NQD, disappeared.

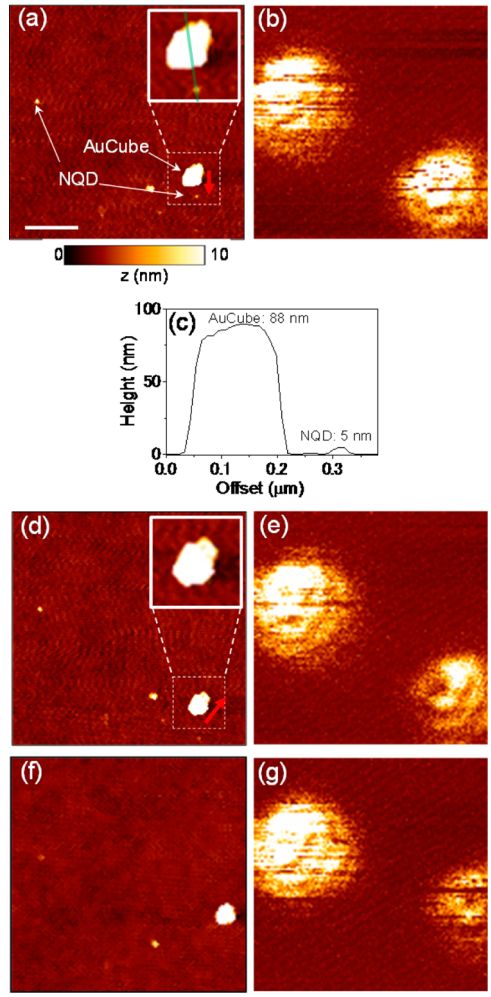

Figure 3. AFM images (a, d, f) and fluorescence images (b, e, g) of the NQD−AuCube system before AFM manipulation of an AuCube (a, b), after AFM manipulation (d, e), and after the AuCube was pushed away from the NQD (f, g). (c) Cross sections of the AuCube and the NQD corresponding to the green line in the inset of (a). In (a) and (d), an AuCube was pushed in the direction indicated by the red arrows. The scale bar in image (a) represents 500 nm.

Subsequently, the AuCube was separated from the single NQD by pushing it in the direction of the arrow to demonstrate that the changes in the fluorescence were reversible. In the AFM image after the AuCube was pushed away (Figure 3f), the single NQD was not visualized, and the position of the fluorescence image of the NQD moved to the upper right (Figure 3g). These observations indicated that the NQD also moved when the AuCube was pushed away. However, it was assumed that the new position of the NQD with respect to the AuCube was of sufficient distance to prevent strong interactions (vide infra). In the fluorescence image, the characteristic blank lines due to the blinking reappeared.

The fluorescence behavior of the single NQD accompanying the above AFM manipulation of the AuCube is summarized in Figure 4. In this measurement, the polarization of the incident laser was aligned vertically in the image. Before moving the AuCube near the NQD, the time trace of the fluorescence intensity (Figure 4a) displayed the well-known fluorescence blinking behavior with distinct on/off periods, which resulted in a bimodal distribution for the corresponding count rate histogram (Figure 4d). The off-state, which is also called the

DOI: 10.1021/acsphotonics.5b00496
ACS Photonics 2016, 3, 109−116

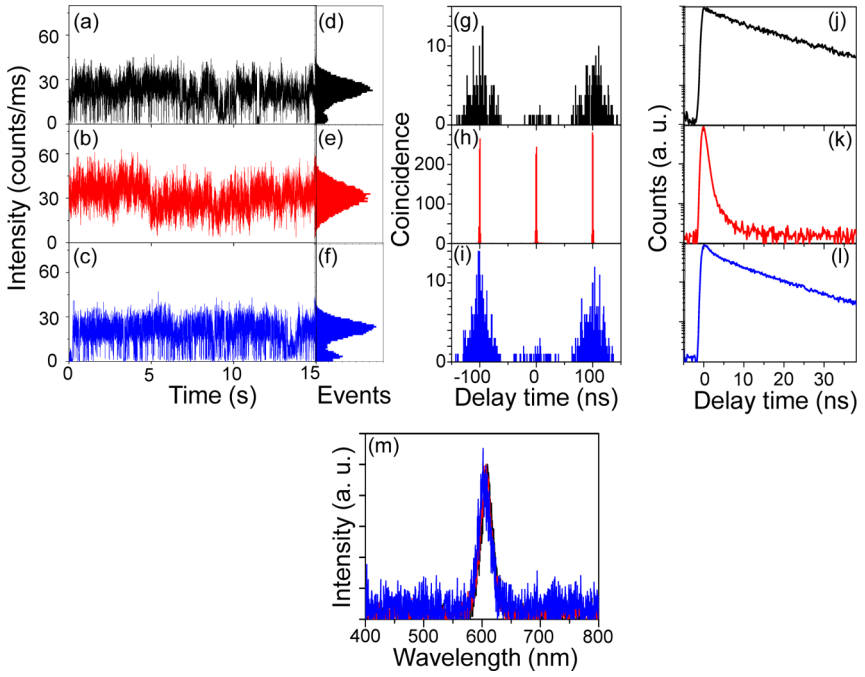

Figure 4. Time traces of fluorescence intensity (a–c), corresponding count rate histograms (d–f), photon correlation histograms (g–i), fluorescence decay curves (j–l), and fluorescence spectra (m) detected from a single NQD before the approach of the AuCube (a, d, g, j, and black line in m) after the approach of the AuCube (b, e, h, k, and red line in m), and after the AuCube was pushed away (c, f, i, l, and blue line in m).

dark-state or the gray-state, results from the quenching of the exciton by the charged state of a NQD that was previously ionized.[46] The quenching process leads to the bimodal distribution in the fluorescence intensity and the multi-exponential fluorescence decay. However, in the case of the single NQD measured here, the quenching was not especially high, and the decay curve (shown in Figure 4j) was well fitted using a single exponential function with a lifetime of 29.6 ns. The maximum fluorescence count of the single NQD was estimated as 47 counts/ms from Figure 4a. In the photon correlation histogram shown in Figure 4g, the contribution of the center peak at a delay time of 0 ns was lower than the other peaks at delay times ±100 ns. In this work, the second-order correlation function, $g^{(2)}(0)$, was defined as the ratio of the number of detection events at the center peak to the average number of detection events at the other peaks. The value of $g^{(2)}(0)$ indicates the probability of a single-photon emission, and this probability increases when $g^{(2)}(0)$ is close to zero. It is known that the $g^{(2)}(0)$ value corresponds to the efficiency of BX emission, Φ_{BX}/Φ_{SX} (Φ_{BX} and Φ_{SX} are QYs of the BX and SX, respectively), at low excitation power, such as with our excitation conditions (the average NQD exciton occupancy $\langle N \rangle \ll 1$).[36,37] The $g^{(2)}(0)$ values were calculated to be 0.14 for Figure 4g, indicating that the individual NQD exhibited single-photon emission, that is, photon antibunching. This fluorescence behavior is characteristic of the single NQD itself and was dramatically changed by interacting with the AuCube.

The fluorescence behavior of the single NQD in proximity of the AuCube is shown in Figure 4b,e,h,k,m. By maneuvering the AuCube close to the single NQD, a reduction of the off-states was observed in the time trace of the fluorescence intensity (Figure 4b). In the count rate histogram (Figure 4e), the reduction of the off-state can be seen in the reduction of the off peak in the bimodal distribution. The maximum fluorescence count of the single NQD increased from 47 to 60 counts/ms. In the photon correlation histogram shown in Figure 4h, the contribution of the center peak increased dramatically, and the $g^{(2)}(0)$ values increased to 0.97. This result indicates that the efficiency of the BX emission from the single NQD was 6.9× higher than that of the single NQD before approaching the AuCube. In Figure 4k, the fluorescence was decayed rapidly, and the two lifetimes of 0.4 ns (99.8%) and 2.5 ns (0.2%) were obtained by fitting the decay curve with a two exponential function. As the lifetime of 0.4 ns is the same as the instrument response function (IRF), the actual lifetime is probably shorter. Therefore, the lifetime was at least 74 times shorter than that of the isolated uncoupled NQD. In Figure 4m, no clear change in the fluorescence spectra was observed by moving the AuCube to near the single NQD. It was reported that the BX emission spectrum was about 15–20 meV red-shifted compared to the SX emission spectrum.[47,48] This energy difference corresponds to 4 to 6 nm red-shift of the BX emission spectrum for the NQD shown in Figure 4m. The full width at half-maximum (fwhm) value of the NQD spectrum before moving the AuCube near the NQD was 21 nm, which was much larger than the spectral shift. Therefore, it is difficult to distinguish the BX emission spectrum from the SX emission spectrum at room temperature. Because neither the emission nor the background scattering from the AuCube were observed in Figure 4m, the increase in the $g^{(2)}(0)$ value and the disappearance of the off-state in the time trace were attributed to the change in the fluorescence behavior of the NQD. By placing the AuCube sufficiently close to the single NQD, the fluorescence intensity increased 1.3×, the efficiency of the BX emission increased 6.9×, and the fluorescence lifetime shortened. This fluorescence behavior is the same as what we reported for AgNPs,[31,32] and the increase in the efficiency of the BX emission is also the same as has been noted in prior reports.[34−39,45] The importance of the above results is that the change in the

DOI: 10.1021/acsphotonics.5b00496
ACS Photonics 2016, 3, 109−116

fluorescence behavior was directly observed by manipulating the distance between an AuCube and a single NQD.

The fluorescence behavior of the single NQD after the AuCube was pushed away is shown in Figure 4c,f,i,l,m. It is clear that the fluorescence intensity, photon antibunching behavior, and decay curve were returned to those detected from the NQD before the approach of the AuCube, i.e., a maximum fluorescence count of 47 counts/ms, the reappearance of the off-state, a $g^{(2)}(0)$ of 0.13, and fluorescence lifetimes of 1.8 ns (23%) and 22.0 ns (77%). The increased off-peak in the count rate histogram, the reduced lifetime (22.0 ns) when compared with the value obtained before the interaction with the AuCube (29.6 ns), and the appearance of an additional short 1.8 ns lifetime may be attributed to changes in the local environment around the NQD. This could indicated that the surface of the NQD was damaged by contact with the AuCube, the NQD was still weakly interacting with the AuCube, or both. The above results directly demonstrate that the efficiency of the BX emission was modified by a shortening of the fluorescence lifetime that resulted from interactions between the AuCube and the single NQD. Although we only show one example here, reproducible results were obtained and can be found in SI.

As mentioned above, the modification of the fluorescence behavior is likely a consequence of an enhancement in the multiexciton relaxation process because an improvement in the excitation process can be eliminated under our excitation conditions. As potential mechanisms for the increased efficiency of BX emission, both an enhancement of the emission rate from the BX state[31,32,34,35,37−39] and a drastic reduction in the Φ_{SX} when compared with the BX,[36,40,41] predominantly by the quenching of the SX, have been reported. In the following, we estimate the AuCube-induced enhancement factors of the radiative and nonradiative (quenching) exciton processes.

By taking into account the enrichments of both excitation and relaxation processes of the NQD, the fluorescence enhancement factor (η_{PL}) is written as

$$\eta_{PL} = \frac{I_p}{I_0} = \frac{\gamma_{exc,p}}{\gamma_{exc,0}}\frac{\Phi_p}{\Phi_0} = \eta_{exc}\frac{\Phi_p}{\Phi_0} \quad (1)$$

where I, γ_{exc}, and Φ represent the fluorescence intensity, the excitation rate, and the fluorescence QY, respectively; the subscript 0 and p refer to the NQD without AuCube and with AuCube, respectively; and $\eta_{exc} = \gamma_{exc,p}/\gamma_{exc,0}$ is the enhancement factor for the excitation rate. The enhancement for the QY is written as

$$\frac{\Phi_p}{\Phi_0} = \frac{k_{rp}}{k_{r0}}\frac{k_{r0} + k_{nr0}}{k_{rp} + k_{nrp}} = \eta_r\frac{\tau_p}{\tau_0} \quad (2)$$

where k_r, k_{nr}, and τ represent radiative and nonradiative decay rates and the fluorescence lifetime, respectively, and $\eta_r = k_{rp}/k_{r0}$ is the enhancement factor for the radiative decay rate. Under our excitation conditions, an enhancement of the excitation rate can probably be eliminated. Hence, η_{exc} should be unity in eq 1. From eqs 1 and 2, the η_r is written as

$$\eta_r \approx \frac{I_p}{I_0}\frac{\tau_0}{\tau_p} \quad (3)$$

It is clear that $\tau_0/\tau_p = \Phi_0\eta_r + (1 - \Phi_0)\eta_{nr}$, where $\eta_{nr} = k_{nrp}/k_{nr0}$ is the enhancement factor for the nonradiative decay rate. Therefore, η_{nr} can be written as

$$\eta_{nr} \approx \frac{(\tau_0/\tau_p) - \Phi_0\eta_r}{1 - \Phi_0} \quad (4)$$

and Φ_0 strongly depends on each individual NQD. When we used $\Phi_0 = 0.5$, as well as $I_0 = 47$ counts/ms, $I_p = 60$ counts/ms, $\tau_0 = 29.6$ ns, and $\tau_p = 0.4$ ns, then the enhancement factors $\eta_r = 95$ and $\eta_{nr} = 54$ were obtained for a single NQD that interacted with an AuCube. As mentioned above, $\tau_p = 0.4$ ns was estimated as the IRF because the decay curve was limited by the IRF. Hence, τ_p is possibly much shorter than 0.4 ns. In this case, the enhancement factors η_r and η_{nr} become larger than 95 and 54, respectively. In addition to the above results, we have four more reproducible results about the fluorescence behavior of a single NQD accompanying the AFM manipulation of an AuCube. The observed fluorescence behavior, that is, the fluorescence intensity, fitting parameters of decay curves, and $g^{(2)}(0)$ before and after the approach of the AuCube, and calculated η_r and η_{nr} about all five NQDs are summarized in Table S1 of SI. Using all results, $\eta_r = 103 \pm 25$ and $\eta_{nr} = 39 \pm 18$ were obtained. The calculated values indicate that both the enhancement of the BX emission rate and the quenching of the SX cause an increase in the efficiency of the BX emission upon the interaction of the NQD with the AuCube. In our results, the fluorescence intensity increased with the efficiency of the BX emission because the emission rate was enhanced by the AuCube, which indicates that the contribution of the enhanced emission rate is greater than the quenching of the SX. This result is quite different from an increase in BX emission resulting from the quenching of SX,[36,40,41] in which the fluorescence intensity would be much lower than that of the isolated uncoupled NQD. Our conclusion is also quite reasonable from the point of view of a reduction in off-states, as observed in the fluorescence time traces. As described above, the off-states were caused by the quenching of SX by the charged NQD which was generated by trapping of an electron of SX and also the AR-assisted ionization (Auger ionization).[22,46] In our case, the BX emission was enhanced by the AuCube and took place before AR could occur. In addition to the enhancement of the BX emission, the quenching of SX occurred, which suppressed the blinking.[40,49,50] Therefore, the off-states in the NQD fluorescence were reduced by the combination of the BX emission enhancement and the quenching of SX. The present results clearly demonstrate that the photon statistics and count rate of the fluorescence from a single NQD can be controlled by modifying the exciton relaxation process using metallic nanostructures.

CONCLUSIONS

We directly demonstrated that the fluorescence behavior of a single NQD can be changed by proximate interactions with an AuCube. By manipulating the AuCube with an AFM manipulation, single-photon emission of the individual NQD was changed to multiphoton emission, and this was accompanied by an increase in the fluorescence intensity and a reduction in the fluorescence lifetime. The fluorescence behavior was then returned to its original state by separating the AuCube from the single NQD. Therefore, these results give direct evidence that single-photon and multiphoton NQD emissions can be modulated by metallic nanostructures. From an estimation of the enhancement factors for radiative and nonradiative (quenching) processes, which were based on the experimental data, the contribution of an increased BX

DOI: 10.1021/acsphotonics.5b00496
ACS Photonics 2016, 3, 109−116

emission rate was greater than that associated with quenching. This in turn led to a BX emission with a higher fluorescence count when the AuCube was observed near the single NQD. It is known that the fluorophore−plasmonic nanostructure interaction strongly depends on the distance between the fluorophore and the plasmonic nanostructure. If it is possible to observe the fluorescence behavior depending on the distance, more knowledge can be obtained. To achieve the observation, the distance has to be controlled in a nanometer-scale precision. In the case of the AFM manipulation technique, however, the distance control was difficult. Therefore, we demonstrated only the changes in the fluorescence behavior accompanying the AFM manipulation. The present findings are important to understand NQD−plasmonic nanostructure interactions, particularly the control of MX dynamics for their efficient use.

METHODS

Commercially available colloidal CdSe/ZnS core/shell NQD (average core radius: 2.6 nm; maximum fluorescence wavelength: 610 nm) were purchased from Invitrogen. Monodisperse cubic Au nanoparticles (AuCube) of a well-defined size and shape were synthesized by a seed-mediated method, as reported in the literature.[51] The sample was prepared by spin-coating an aqueous AuCube dispersion and then a toluene solution of colloidal CdSe/ZnS NQDs onto a clean glass coverslip.

In situ manipulation of an AuCube and the detection of the fluorescence from a single NQD was realized by a home-built AFM (NanoWizard II, JPK instruments)/inverted confocal microscope (IX-71, Olympus) system (Figure 1). In addition to the three closed-loop piezo-driven axes of the AFM, a two axis, closed-loop, piezo-driven sample stage was employed. A linearly polarized pulsed laser beam (405 nm, 10.0 MHz, 90 ps fwhm, PicoQuant) with a power of 57 W/cm^2 was used as an excitation light source with the inverted microscope, and it was focused to a diffraction-limited spot on the sample by an objective lens (NA 1.4, Olympus). The number of excitons generated in a single NQD by a single excitation pulse was estimated to be 0.10 by taking into account the absorption cross-section of the NQD and the number of photons in a single excitation pulse. The fluorescence photons from the NQD were collected by the same objective lens and passed through a confocal pinhole and a long-pass filter to remove the excitation laser. Subsequently, half of the photons were detected by a spectrograph (SpectraPro2358, Acton Research Corporation) with a cooled CCD camera (PIXIS400B, Princeton Instruments). The remaining half of the photons were passed through a band-pass filter and were detected by two avalanche single-photon counting modules (SPCM-AQR-14, PerkinElmer) for Hanbury-Brown and Twiss-type photon correlation (HBT) and lifetime measurements. The time-resolution of the lifetime measurement (instrument response function: IRF) was approximately 0.4 ns. Details can be found in the SI.

The manipulation of a single AuCube and the detection of the fluorescence behavior of a single NQD were performed by the following procedure. Initially, a silicon AFM tip was coupled to the center of a focused excitation laser by the piezo of the AFM. Then, AFM topography and fluorescence images of the sample were measured simultaneously by scanning the sample stage. By choosing a fluorescence spot corresponding to the single NQD, the fluorescence behavior of the single NQD was measured before AFM manipulation. A single AuCube was then moved to the individual NQD using the AFM tip and translating the sample stage. The AFM topography image was obtained, and the fluorescence behavior of the single NQD coupled to the AuCube was measured. Then, the AuCube was separated from the single NQD, and the fluorescence behavior of the single NQD was measured again. AFM topography measurement and AFM manipulation of the AuCube were performed in tapping and contact modes, respectively. All measurements were performed at room temperature under ambient conditions.

ASSOCIATED CONTENT

Supporting Information

The Supporting Information is available free of charge on the ACS Publications website at DOI: 10.1021/acsphotonics.5b00496.

Instrumental setup, AFM image of AuCube and scanning electron microscopy images of an AFM tip, fluorescence behavior of a single NQD accompanying the AFM manipulation of au AuCube (PDF).

AUTHOR INFORMATION

Corresponding Author

*E-mail: masuo@kwansei.ac.jp.

Notes

The authors declare no competing financial interest.

ACKNOWLEDGMENTS

This work was partly supported by a Grant-in-Aid for Scientific Research (No. 26390023) from the Japan Society for the Promotion of Science (JSPS) and a Grant-in-Aid for Scientific Research on Innovation Areas “Photosynergetics” (No. 26107005) from MEXT, Japan.

ABBREVIATIONS

colloidal nanocrystal quantum dot:NQD; atomic force microscopy:AFM; cubic gold nanoparticle:AuCube; multiple excitons:MX; triexciton:TX; biexciton:BX; single exciton:SX; multiple exciton generation:MEG; Auger recombination:AR; silver nanoparticles:AgNPs; quantum yield:QY; instrument response function:IRF; transmission electron microscopy:-TEM; localized surface plasmon resonance:LSPR; Hanbury-Brown and Twiss-type photon correlation:HBT

REFERENCES

(1) Klein, D. L.; Roth, R.; Lim, A. K. L.; Alivisatos, A. P.; McEuen, P. L. A single-electron transistor made from a cadmium selenide nanocrystal. *Nature* **1997**, *389*, 699−701.

(2) Klimov, V. I.; Mikhailovsky, A. A.; Xu, S.; Malko, A.; Hollingsworth, J. A.; Leatherdale, C. A.; Eisler, H.; Bawendi, M. G. Optical gain and stimulated emission in nanocrystal quantum dots. *Science* **2000**, *290*, 314−317.

(3) Coe, S.; Woo, W. K.; Bawendi, M.; Bulovic, V. Electroluminescence from single monolayers of nanocrystals in molecular organic devices. *Nature* **2002**, *420*, 800−803.

(4) Klimov, V. I. Mechanisms for photogeneration and recombination of multiexcitons in semiconductor nanocrystals: implications for lasing and solar energy conversion. *J. Phys. Chem. B* **2006**, *110*, 16827−16845.

(5) Robel, I.; Subramanian, V.; Kuno, M.; Kamat, P. V. Quantum dot solar cells. harvesting light energy with CdSe nanocrystals molecularly

DOI: 10.1021/acsphotonics.5b00496
ACS Photonics 2016, 3, 109−116

linked to mesoscopic TiO_2 films. *J. Am. Chem. Soc.* **2006**, *128*, 2385−2393.
(6) Klimov, V. I.; Ivanov, S. A.; Nanda, J.; Achermann, M.; Bezel, I.; McGuire, J. A.; Piryatinski, A. Single-exciton optical gain in semiconductor nanocrystals. *Nature* **2007**, *447*, 441−446.
(7) Kamat, P. V. Quantum Dot Solar Cells. Semiconductor Nanocrystals as Light Harvesters. *J. Phys. Chem. C* **2008**, *112*, 18737−18753.
(8) Qian, L.; Zheng, Y.; Xue, J. G.; Holloway, P. H. Stable and efficient quantum-dot light-emitting diodes based on solution-processed multilayer structures. *Nat. Photonics* **2011**, *5*, 543−548.
(9) Bourzac, K. Quantum dots go on display. *Nature* **2013**, *493*, 283.
(10) Schaller, R. D.; Klimov, V. I. High efficiency carrier multiplication in PbSe nanocrystals: implications for solar energy conversion. *Phys. Rev. Lett.* **2004**, *92*, 186601.
(11) Ellingson, R. J.; Beard, M. C.; Johnson, J. C.; Yu, P.; Micic, O. I.; Nozik, A. J.; Shabaev, A.; Efros, A. L. Highly efficient multiple exciton generation in colloidal PbSe and PbS quantum dots. *Nano Lett.* **2005**, *5*, 865−871.
(12) Schaller, R. D.; Agranovich, V. M.; Klimov, V. I. High-efficiency carrier multiplication through direct photogeneration of multi-excitons via virtual single-exciton states. *Nat. Phys.* **2005**, *1*, 189−194.
(13) Murphy, J. E.; Beard, M. C.; Norman, A. G.; Ahrenkiel, S. P.; Johnson, J. C.; Yu, P. R.; Micic, O. I.; Ellingson, R. J.; Nozik, A. J. PbTe colloidal nanocrystals: Synthesis, characterization, and multiple exciton generation. *J. Am. Chem. Soc.* **2006**, *128*, 3241−3247.
(14) Beard, M. C.; Knutsen, K. P.; Yu, P.; Luther, J. M.; Song, Q.; Metzger, W. K.; Ellingson, R. J.; Nozik, A. J. Multiple Exciton Generation in Colloidal Silicon Nanocrystals. *Nano Lett.* **2007**, *7*, 2506−2512.
(15) Nozik, A. J. Quantum dot solar cells. *Phys. E* **2002**, *14*, 115−120.
(16) Law, M.; Beard, M. C.; Choi, S.; Luther, J. M.; Hanna, M. C.; Nozik, A. J. Determining the Internal Quantum Efficiency of PbSe Nanocrystal Solar Cells with the Aid of an Optical Model. *Nano Lett.* **2008**, *8*, 3904−3910.
(17) Pattantyus-Abraham, A. G.; Kramer, I. J.; Barkhouse, A. R.; Wang, X. H.; Konstantatos, G.; Debnath, R.; Levina, L.; Raabe, I.; Nazeeruddin, M. K.; Gratzel, M.; Sargent, E. H. Depleted-Heterojunction Colloidal Quantum Dot Solar Cells. *ACS Nano* **2010**, *4*, 3374−3380.
(18) Semonin, O. E.; Luther, J. M.; Choi, S.; Chen, H. Y.; Gao, J. B.; Nozik, A. J.; Beard, M. C. Peak External Photocurrent Quantum Efficiency Exceeding 100% via MEG in a Quantum Dot Solar Cell. *Science* **2011**, *334*, 1530−1533.
(19) Tang, J. A.; Sargent, E. H. Infrared Colloidal Quantum Dots for Photovoltaics: Fundamentals and Recent Progress. *Adv. Mater.* **2011**, *23*, 12−29.
(20) Benson, O.; Santori, C.; Pelton, M.; Yamamoto, Y. Regulated and Entangled Photons from a Single Quantum Dot. *Phys. Rev. Lett.* **2000**, *84*, 2513.
(21) Klimov, V. V.; Mikhailovsky, A. A.; McBranch, D. W.; Leatherdale, C. A.; Bawendi, M. G. Quantization of multiparticle auger rates in semiconductor quantum dots. *Science* **2000**, *287*, 1011−1013.
(22) Efros, A. L.; Rosen, M. Random Telegraph Signal in the Photoluminescence Intensity of a Single Quantum Dot. *Phys. Rev. Lett.* **1997**, *78*, 1110.
(23) Htoon, H.; Malko, A. V.; Bussian, D.; Vela, J.; Chen, Y.; Hollingsworth, J. A.; Klimov, V. I. Highly emissive multiexcitons in steady-state photoluminescence of individual "giant" CdSe/CdS Core/Shell nanocrystals. *Nano Lett.* **2010**, *10*, 2401−2407.
(24) Osovsky, R.; Cheskis, D.; Kloper, V.; Sashchiuk, A.; Kroner, M.; Lifshitz, E. Continuous-wave pumping of multiexciton bands in the photoluminescence spectrum of a single CdTe-CdSe core-shell colloidal quantum dot. *Phys. Rev. Lett.* **2009**, *102*, 197401.
(25) Wang, X. Y.; Ren, X. F.; Kahen, K.; Hahn, M. A.; Rajeswaran, M.; Maccagnano-Zacher, S.; Silcox, J.; Cragg, G. E.; Efros, A. L.; Krauss, T. D. Non-blinking semiconductor nanocrystals. *Nature* **2009**, *459*, 686−689.
(26) Garcia-Santamaria, F.; Chen, Y.; Vela, J.; Schaller, R. D.; Hollingsworth, J. A.; Klimov, V. I. Suppressed auger recombination in "giant" nanocrystals boosts optical gain performance. *Nano Lett.* **2009**, *9*, 3482−3488.
(27) Lounis, B.; Bechtel, H. A.; Gerion, D.; Alivisatos, P.; Moerner, W. E. Photon antibunching in single CdSe/ZnS quantum dot fluorescence. *Chem. Phys. Lett.* **2000**, *329*, 399−404.
(28) Michler, P.; Imamoglu, A.; Mason, M. D.; Carson, P. J.; Strouse, G. F.; Buratto, S. K. Quantum correlation among photons from a single quantum dot at room temperature. *Nature* **2000**, *406*, 968−970.
(29) Messin, G.; Hermier, J. P.; Giacobino, E.; Desbiolles, P.; Dahan, M. Bunching and antibunching in the fluorescence of semiconductor nanocrystals. *Opt. Lett.* **2001**, *26*, 1891−1893.
(30) Brokmann, X.; Giacobino, E.; Dahan, M.; Hermier, J. P. Highly efficient triggered emission of single photons by colloidal CdSe/ZnS nanocrystals. *Appl. Phys. Lett.* **2004**, *85*, 712−714.
(31) Masuo, S.; Naiki, H.; Machida, S.; Itaya, A. Photon statistics in enhanced fluorescence from a single CdSe/ZnS quantum dot in the vicinity of silver nanoparticles. *Appl. Phys. Lett.* **2009**, *95*, 193106.
(32) Naiki, H.; Masuo, S.; Machida, S.; Itaya, A. Single-Photon Emission Behavior of Isolated CdSe/ZnS Quantum Dots Interacting with the Localized Surface Plasmon Resonance of Silver Nanoparticles. *J. Phys. Chem. C* **2011**, *115*, 23299−23304.
(33) Masuo, S.; Tanaka, T.; Machida, S.; Itaya, A. Photon antibunching in enhanced photoluminescence of a single CdSe/ZnS nanocrystal by silver nanostructures. *J. Photochem. Photobiol., A* **2012**, *237*, 24−30.
(34) Canneson, D.; Mallek-Zouari, I.; Buil, S.; Quelin, X.; Javaux, C.; Mahler, B.; Dubertret, B.; Hermier, J. P. Strong Purcell effect observed in single thick-shell CdSe/CdS nanocrystals coupled to localized surface plasmons. *Phys. Rev. B: Condens. Matter Mater. Phys.* **2011**, *84*, 245423.
(35) Park, Y.-S.; Ghosh, Y.; Xu, P.; Mack, N. H.; Wang, H.-L.; Hollingsworth, J. A.; Htoon, H. Single-Nanocrystal Photoluminescence Spectroscopy Studies of Plasmon−Multiexciton Interactions at Low Temperature. *J. Phys. Chem. Lett.* **2013**, *4*, 1465−1470.
(36) Park, Y.-S.; Ghosh, Y.; Chen, Y.; Piryatinski, A.; Xu, P.; Mack, N. H.; Wang, H.-L.; Klimov, V. I.; Hollingsworth, J. A.; Htoon, H. Super-Poissonian Statistics of Photon Emission from Single CdSe-CdS Core-Shell Nanocrystals Coupled to Metal Nanostructures. *Phys. Rev. Lett.* **2013**, *110*, 117401.
(37) Wang, F.; Karan, N. S.; Nguyen, H. M.; Ghosh, Y.; Sheehan, C. J.; Hollingsworth, J. A.; Htoon, H. Correlated structural-optical study of single nanocrystals in a gap-bar antenna: effects of plasmonics on excitonic recombination pathways. *Nanoscale* **2015**, *7*, 9387−9393.
(38) Leblanc, S. J.; McClanahan, M. R.; Jones, M.; Moyer, P. J. Enhancement of Multiphoton Emission from Single CdSe Quantum Dots Coupled to Gold Films. *Nano Lett.* **2013**, *13*, 1662−1669.
(39) Yuan, C. T.; Wang, Y. C.; Cheng, H. W.; Wang, H. S.; Kuo, M. Y.; Shih, M. H.; Tang, J. Modification of Fluorescence Properties in Single Colloidal Quantum Dots by Coupling to Plasmonic Gap Modes. *J. Phys. Chem. C* **2013**, *117*, 12762−12768.
(40) Cheng, H. W.; Yuan, C. T.; Wang, J. S.; Lin, T. N.; Shen, J. L.; Hung, Y. J.; Tang, J.; Tseng, F. G. Modification of Photon Emission Statistics from Single Colloidal CdSe Quantum Dots by Conductive Materials. *J. Phys. Chem. C* **2014**, *118*, 18126−18132.
(41) Gao, Y.; Roslyak, O.; Dervishi, E.; Karan, N. S.; Ghosh, Y.; Sheehan, C. J.; Wang, F.; Gupta, G.; Mohite, A.; Dattelbaum, A. M.; Doorn, S. K.; Hollingsworth, J. A.; Piryatinski, A.; Htoon, H. Hybrid Graphene-Giant Nanocrystal Quantum Dot Assemblies with Highly Efficient Biexciton Emission. *Adv. Opt. Mater.* **2015**, *3*, 39−43.
(42) Bek, A.; Jansen, R.; Ringler, M.; Mayilo, S.; Klar, T. A.; Feldmann, J. Fluorescence enhancement in hot spots of AFM-designed gold nanoparticle sandwiches. *Nano Lett.* **2008**, *8*, 485−490.
(43) Schietinger, S.; Barth, M.; Aichele, T.; Benson, O. Plasmon-Enhanced Single Photon Emission from a Nanoassembled Metal-Diamond Hybrid Structure at Room Temperature. *Nano Lett.* **2009**, *9*, 1694−1698.

DOI: 10.1021/acsphotonics.5b00496
ACS Photonics 2016, 3, 109−116

(44) Huck, A.; Kumar, S.; Shakoor, A.; Anderson, U. L. Controlled Coupling of a Single Nitrogen-Vacancy Center to a Silver Nanowire. *Phys. Rev. Lett.* **2011**, *106*, 096801.
(45) Ratchford, D.; Shafiei, F.; Kim, S.; Gray, S. K.; Li, X. Manipulating Coupling between a Single Semiconductor Quantum Dot and Single Gold Nanoparticle. *Nano Lett.* **2011**, *11*, 1049−1054.
(46) Galland, C.; Ghosh, Y.; Steinbruck, A.; Sykora, M.; Hollingsworth, J. A.; Klimov, V. I.; Htoon, H. Two types of luminescence blinking revealed by spectroelectrochemistry of single quantum dots. *Nature* **2011**, *479*, 203−208.
(47) Achermann, M.; Hollingsworth, J. A.; Klimov, V. I. Multi-excitons confined within a subexcitonic volume: Spectroscopic and dynamical signatures of neutral and charged biexcitons in ultrasmall semiconductor nanocrystals. *Phys. Rev. B: Condens. Matter Mater. Phys.* **2003**, *68*, 245302.
(48) Fisher, B.; Caruge, J. M.; Zehnder, D.; Bawendi, M. Room-temperature ordered photon emission from multiexciton states in single CdSe core-shell nanocrystals. *Phys. Rev. Lett.* **2005**, *94*, 087403.
(49) Matsumoto, Y.; Kanemoto, R.; Itoh, T.; Nakanishi, S.; Ishikawa, M.; Biju, V. Photoluminescence quenching and intensity fluctuations of CdSe-ZnS quantum dots on an Ag nanoparticle film. *J. Phys. Chem. C* **2008**, *112*, 1345−1350.
(50) Hamada, M.; Nakanishi, S.; Itoh, T.; Ishikawa, M.; Biju, V. Blinking suppression in CdSe/ZnS single quantum dots by TiO2 nanoparticles. *ACS Nano* **2010**, *4*, 4445−4454.
(51) Eguchi, M.; Mitsui, D.; Wu, H. L.; Sato, R.; Teranishi, T. Simple reductant concentration-dependent shape control of polyhedral gold nanoparticles and their plasmonic properties. *Langmuir* **2012**, *28*, 9021−9026.

DOI: 10.1021/acsphotonics.5b00496
ACS Photonics 2016, 3, 109−116